energies

MDPI

Article

Model Test and Sea Trial of a Multi-Absorber 1 MW Wave Energy Converter

Min Chen [1,2], Songwei Sheng [1,2,*], Yaqun Zhang [1,2], Zhenpeng Wang [1,2], Kunlin Wang [1,2] and Jiaqiang Jiang [1,2]

[1] Guangzhou Institute of Energy Conversion, Chinese Academy of Sciences, Guangzhou 510640, China; chenmin@ms.giec.ac.cn (M.C.); zhangyq@ms.giec.ac.cn (Y.Z.); wangzp@ms.giec.ac.cn (Z.W.); wangkl@ms.giec.ac.cn (K.W.); jiangjq@ms.giec.ac.cn (J.J.)
[2] Guangdong Provincial Key Laboratory of Renewable Energy, Guangzhou 510640, China
* Correspondence: shengsw@ms.giec.ac.cn

Abstract

An innovative multi-absorber 1 MW wave energy converter (WEC), Nankun, is proposed for efficient wave energy extraction. It comprises a semi-submersible floating platform, a wave energy capture mechanism, a hydraulic energy conversion system, and a mooring system. The WEC operates by converting fluctuating wave power into stable electrical output through a unique sharp eagle-shaped wave absorber coupled with a hydraulic energy conversion module. Scaled model experiments (1:25) demonstrated energy-capture efficiency ranges predominantly between 30% and 50% across 0.8–1.4 s wave periods, with a peak of 56.17%. Analysis of the wave direction effect revealed that the device achieved significantly a higher energy capture at 180 deg compared with 0 deg wave headings, with a relative efficiency ratio of approximately 1.0:0.6~0.8. A full-scale prototype with 10 absorbers was deployed in the South China Sea, achieving grid connection in November 2023. Operational data confirmed viability and generation capacity, with the peak daily output reaching 9850 kWh and a cumulative production of 89,852 kWh over 20 days.

Keywords: wave energy; multi-absorber 1 MW WEC; energy capture efficiency; wave direction effect; model test; sea trial

Academic Editor: Duarte Valério

Received: 23 July 2025
Revised: 29 August 2025
Accepted: 2 September 2025
Published: 4 September 2025

Citation: Chen, M.; Sheng, S.; Zhang, Y.; Wang, Z.; Wang, K.; Jiang, J. Model Test and Sea Trial of a Multi-Absorber 1 MW Wave Energy Converter. *Energies* **2025**, *18*, 4711. https://doi.org/10.3390/en18174711

1. Introduction

With advancing industrialization and growing energy demands, global reliance on renewable sources has intensified [1,2]. Wave energy harvesting offers distinct advantages over wind and solar power due to its higher energy density (3 kW/m^2 [3], 0.5 kW/m^2 [3], and 0.17 kW/m^2 [4], respectively), broad distribution, and persistent availability [5]. Global wave energy resource reserves, estimated at 29,500 TWh/year, underscore its potential [6,7]. Consequently, wave energy converters (WECs) have become a focal point in marine renewable energy research. The main challenges currently facing wave energy technology are the high levelized cost of energy (LCOE), stemming from the survivability design for extreme sea conditions, high installation and operations and maintenance costs, and the lack of standardized technological pathways [4]. Therefore, the novel multi-body WEC design proposed in this study aims to explore new solutions in terms of reliability and cost-effectiveness to address these challenges.

Based on the working principle, WECs are broadly classified into three categories: overtopping (OP), oscillating water column (OWC), and oscillating buoy (OB) systems [8,9]. OP devices employ ramps to lift waves overtop and channel waves into reservoirs, and subsequent seawater returns through low-head turbines, which generate power via hydraulic

potential differences. Early implementations include the 350 kW Tapchan plant installed on shore at Toftestallen, Norway, in the 1980s [10,11] and the 57 m long and 27 m wide and 237 tons heavy Wave Dragon prototype placed in Denmark in 2003 [12–14]. Wave Dragon's scalable design enables unit capacities from 1.5 to 19 MW, sized according to local wave climates. An OP device's performance hinges critically on ramp geometry and reservoir inflow dynamics [15,16], leading to innovations like the multi-reservoir Sea-wave Slot-cone Generator (SSG) in Norway [17–20].

OWC WECs convert wave motions into oscillating air columns within submerged chambers, driving turbines via reciprocating airflow [21]. Originating from 19th-century navigation whistling buoys [8,22], modern OWCs emerged from Yoshio Masuda's buoy designs in the 1940s, which were deployed in Osaka Bay and delivered a small output (70–500 W) [23]. In the 1990s and 2000s, several full-scale OWC WECs were built and tested. The milestone is the shoreline prototype LIMPET, with a capacity of 75 kW, on Islay Island in 1991 [24,25]. It was decommissioned after ten years of operation spanning 1991–2000. Then, the 500 kW LIMPET successor was developed and operated from 2000 to 2018 [8,24,25]. The LIMPET successfully demonstrated the commercialization of OWC technology. Another visible achievement is the floating Mighty Whale WEC, with a capacity of approximately 110 kW, developed by the Japanese company MIGHTY in 1998 [26,27]. It was installed at a depth of 40 m in the mouth of Gokasho Bay in Japan and moored by a six-mooring-line system. The Backward Bent Duct Buoy (BBDB) is an alternative concept optimized for shallow waters, since it comprises an L-shaped OWC instead of a vertical central tube [24,28]. The BBDB achieved deployment milestones such as the 500 kW OE Buoy in Galway Bay, Ireland, in 2008, and the 1.25 MW off the coast of Hawaii in 2024.

Despite their prominence, OP and OWC systems face significant limitations. OP devices suffer from low efficiency, site constraints, and high construction costs, while OWC devices contend with turbine inefficiency, turbine structural durability, and high operating expenses [23]. In contrast, OB WECs achieve superior energy capture across broadband wave conditions through the buoys' responsive motion, translating wave energy into mechanical energy. Their modular design enables scalable deployments of wave farms, and their mechanical simplicity reduces maintenance costs [29]. Additionally, the adaptable design configurations of OB WECs permit installation in both nearshore and offshore environments, offering exceptional deployment flexibility.

A typical OB WEC is the point absorber PowerBuoy 150 kW in the USA [30]. It collects energy by converting the up-and-down motion of waves into the heaving motion of the buoy. The WaveStar is a floating multi-body, which could be equipped with a maximum of 20 floats. Waves run the length of the machine, lifting 20 floats in turn to power the motor [31,32]. The pendulum-type Oyster encompasses a mechanical surface piercing flap hinged to a base structure mounted on the seabed. The flap is positioned perpendicular to wave direction, and sways with waves driving hydraulic pistons [33]. At the European Marine Energy Centre's wave energy test site, Aquamarine Power deployed and tested the 315 kW Oyster 1 from 2009 to 2012 and the 800 kW Oyster 800 from 2012 to 2015. The Pelamis 750 kW prototype converter is a unique articulated-cylinder device. Waves perform work on the Pelamis by moving adjacent cylinders relative to each other [34]. The world's first array and wave farm of three Pelamis P1 wave energy devices (750 kW capacity each; 135 m long and 3.5 m wide connected cylinders ride and fall with the waves) was deployed off the Atlantic coastline of northern Portugal in 2008 [35]. More recently, the Guangzhou Institute of Energy Conversion developed a series of sharp eagle-shaped WECs, including the 10 kW Eagle One, 100 kW Wanshan, 260 kW Pilot One, and 500 kW Zhoushan [36–38]. The sharp eagle-shaped WECs exemplified OB efficiency through specialized wave absorber-driving hydraulic generators.

Nevertheless, existing OB WECs remain confined to kilowatt-scale capacities (10–800 kW), with high per-kilowatt costs and suboptimal spatial efficiency. Advancing megawatt-scale OB systems, integrated with complementary renewables like solar, is thus critical to achieving cost reduction, efficiency improvement, and optimized ocean-space utilization.

This study proposed an innovative multi-absorber 1 MW WEC Nankun derived from sharp eagle-shaped technology and augmented with 250 kW solar capabilities (photovoltaic panels on its deck). Section 2 details the device design and working principle. Section 3 describes experimental methods, including wave tank, model, and instrumentation. Section 4 analyses energy-capture efficiency and directional wave effects. Section 5 discusses prototype construction and sea trial results. Conclusions are summarized in Section 6.

2. Design and Working Principle

The 1 MW WEC Nankun comprises four primary subsystems: a semi-submersible floating platform, a wave energy capture mechanism, a hydraulic energy conversion system, and a mooring system.

As illustrated in Figure 1, the semi-submersible platform features a three-column structure with interconnected lower pontoons, serving as the structural foundation for the wave energy capture and conversion systems. The device is moored by a chain mooring system. The mooring system is composed of three bundles. Each bundle comprises two mooring lines. The angular spacing between bundles is 120 deg.

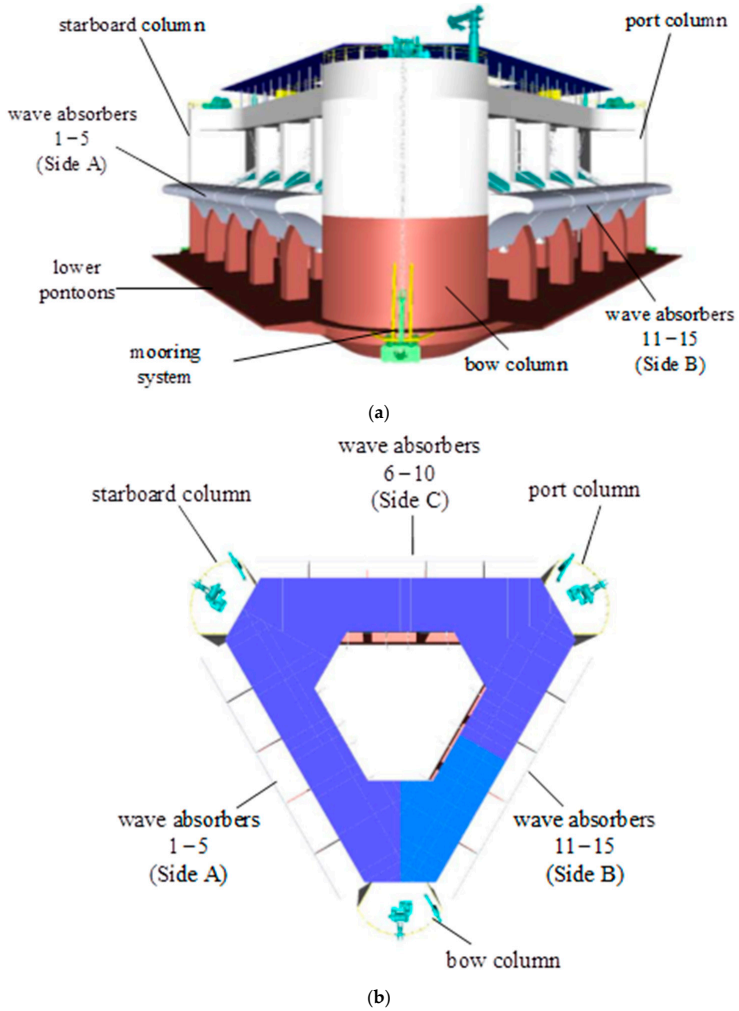

Figure 1. Schematic illustration of the 1 MW WEC: (**a**) front view; (**b**) plan view.

The wave energy capture mechanism consists of 15 sharp eagle-shaped wave absorbers positioned between each pair of columns on three sides of the platform. Each absorber is mechanically linked to the platform via two A-frame support shafts (providing rotational stability) and a hydraulic cylinder mounted atop (enabling energy transfer). The wave absorbers are distributed as follows:

- Wave absorbers 1–5: installed between the bow and starboard columns;
- Wave absorbers 6–10: positioned between the starboard and port columns;
- Wave absorbers 11–15: located between the port and bow columns.

With all units numbered clockwise for systematic reference. A mooring system ensures station-keeping, allowing the WEC to operate safely under specified environmental conditions while maintaining optimal energy-capture efficiency.

The top deck of the semi-submersible platform is equipped with photovoltaic panels for solar power generation, with a PV-installed capacity of 250 kW. The device integrates both wave energy and solar power generation.

The hydraulic energy conversion system comprises a hydraulic cylinder, accumulator, control valve, tank, hydraulic motor, and generator. As shown in Figure 2, the energy conversion process occurs in three sequential stages:

(1) Wave-to-mechanical conversion:

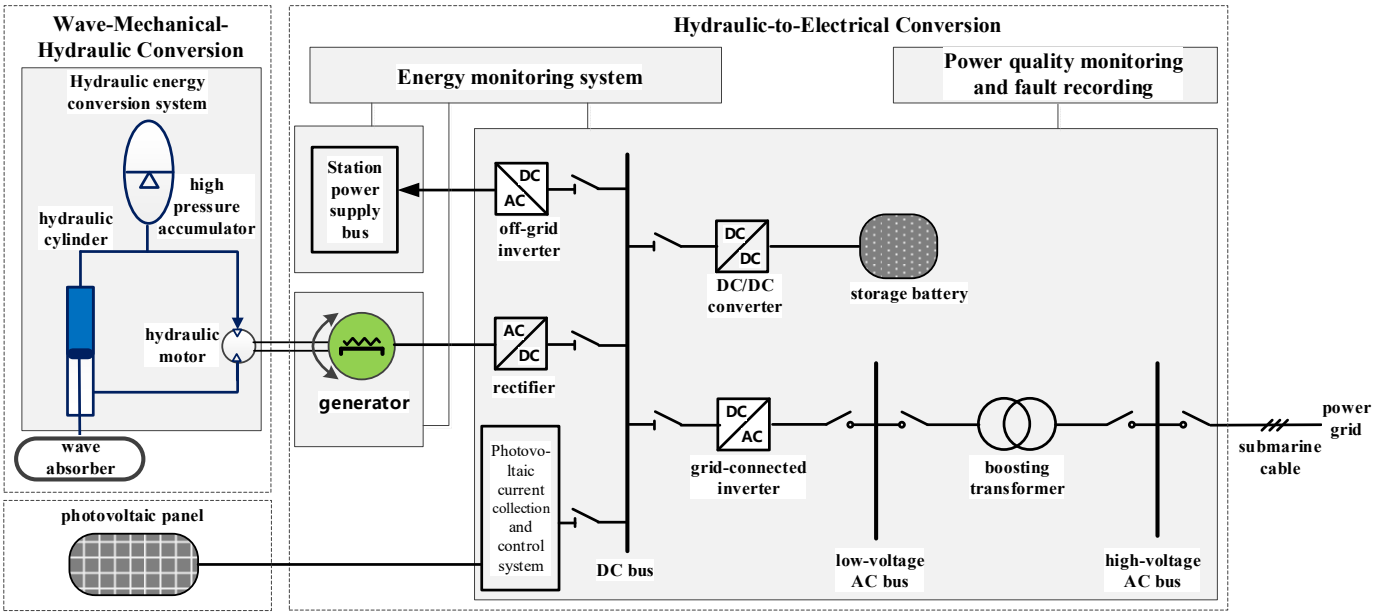

Figure 2. Schematic diagram of the energy conversion process.

Each wave absorber undergoes a single degree of freedom oscillatory motion in response to wave excitation, driving the attached hydraulic cylinder in a reciprocating linear motion. This stage transduces wave energy into mechanical energy.

(2) Mechanical-to-hydraulic conversion:

The hydraulic cylinder pressurizes and discharges hydraulic fluid into a high-pressure accumulator, thereby converting mechanical energy into stored hydraulic energy.

(3) Hydraulic-to-electrical conversion:

Once fluid pressure reaches a predefined threshold, the high-pressure oil is released through a control valve, driving a hydraulic motor coupled to an electric generator. Brief intervals of no power generation may occur as pressure builds up to the threshold. This

design decouples the power generation from the fluctuating and intermittent wave input, significantly reducing power generation interruptions caused by wave troughs or low-energy wave conditions. During hydraulic pressure decreases, the output torque of the hydraulic motor decreases. To maintain a constant motor speed, the electromagnetic torque is actively regulated via generator control to achieve continuous matching with the hydraulic motor's output torque. This final stage completes the energy conversion chain, yielding electrical power. The hydraulic power from multiple wave absorbers is converted to electricity and then aggregated.

Figure 2 also shows how the DC power generated by the photovoltaic (PV) panels is fed into the common DC bus, where it is combined with the DC power produced by the wave energy system's rectifiers. The central control system and the unified DC/AC inverter manages the combined power from the DC bus and ensures a grid-compliant output.

The 1 MW WEC Nankun is compared with other OB WECs in Table 1. The installed capacity, working principle, movement type, Power Take-Off (PTO) system and the energy-capture efficiency are selected as five indicators for further analysis. Nankun has the largest installed capacity, which is of great significance for reducing the LCOE. According to the shape, size, and angle of the relative incident wave direction of the absorber, the OB WEC can be divided into three types: a point absorber, attenuator, and terminator. As a terminator type, Nankun has a higher energy-capture efficiency compared with point absorber and attenuator types. In particular, it has multiple absorbers and a three-fold symmetric layout, which enables it to absorb waves from all directions. Moreover, it is integrated with complementary solar energy. Hence, it has potential advantages over traditional OB WECs in terms of structural cost, power smoothing, directional adaptability, and integrated energy utilization rate.

Table 1. Comparison of parameters of several OB WECs.

Name	Installed Capacity	Working Principle	Movement Type	PTO System	Efficiency (%)
PowerBuoy [39]	150 kW	Point absorber	Heave	Hydraulic type	20
AquaBuoy [40]	250 kW	Point absorber	Heave	Turbine	20
WaveStar [31]	110 kW	Point absorber	Heave	Hydraulic type	25
Pelamis [41]	750 kW	Attenuator	Angular displacement	Hydraulic type	15
Oyster [42]	800 kW	Terminator	Swing	Hydraulic type	40
Wanshan [38]	100 kW	Terminator	Pitch	Hydraulic type	43
Nankun	1 MW	Terminator	Pitch	Hydraulic type	56

3. Model Test

3.1. Towing Tank Facility

Hydrodynamic tests of the 1 MW WEC were conducted in the State Key Laboratory of Ocean Engineering at Shanghai Jiao Tong University. The towing tank is 300 m long, 16 m wide and 7.5 m deep. It features a multi-unit wave generation system capable of simulating regular and irregular waves (maximum wave height of 0.55 m). Wave conditions were generated by controlling the amplitude and period of the wave maker's paddles. Passive wave absorption was achieved through perforated crate end/sidewalls for energy dissipation.

3.2. WEC Model

The model test used a geometric scale ratio of 1:25. As the performance of the WEC was primarily governed by gravitational and inertial forces, the model test followed Froude's law of similarity. According to this law, the scaling relationships for physical quantities between the model and the prototype are shown in Table 2. λ = 25 is the linear scale ratio of the model and γ is the density ratio of seawater to fresh water.

Table 2. Scaling relationships for physical quantities between the model and the prototype.

Parameter	Symbol	Scale Ratio
Leng	L_s/L_m	λ
Time	T_s/T_m	$\lambda^{1/2}$
Velocity	V_s/V_m	$\lambda^{1/2}$
Force	F_s/F_m	$\gamma\lambda^3$
Power	P_s/P_m	$\gamma\lambda^{3.5}$

Froude's law of similarity also has its limitations, namely that the Reynolds number effects (related to viscous drag) are not correctly scaled. However, for the large-volume structure l MW WEC, the hydrodynamic forces are dominated by form drag and wave radiation damping, both of which are correctly modeled under Froude scaling. Therefore, the viscous effects are considered secondary, and the model test results are deemed to have high transferability to the full-scale facility.

Main dimensions of the 1 MW WEC Nankun are listed in Table 3. A scaled model (1:25 ratio) was fabricated, comprising a semi-submersible platform and sharp eagle-shaped wave absorbers, as shown in Figure 3a.

Table 3. Principal dimensions of the 1 MW WEC Nankun.

Parameter	Prototype	Model
Column diameter (m)	9.5	0.38
Distance between columns (m)	60	2.40
Pontoon height (m)	4	0.16
Operation freeboard (m)	10.5	0.42
Operation draft (m)	13.5	0.54
Single wave absorber width (m)	11.7	0.47
Displacement (kg)	18,155,000	1,133,580

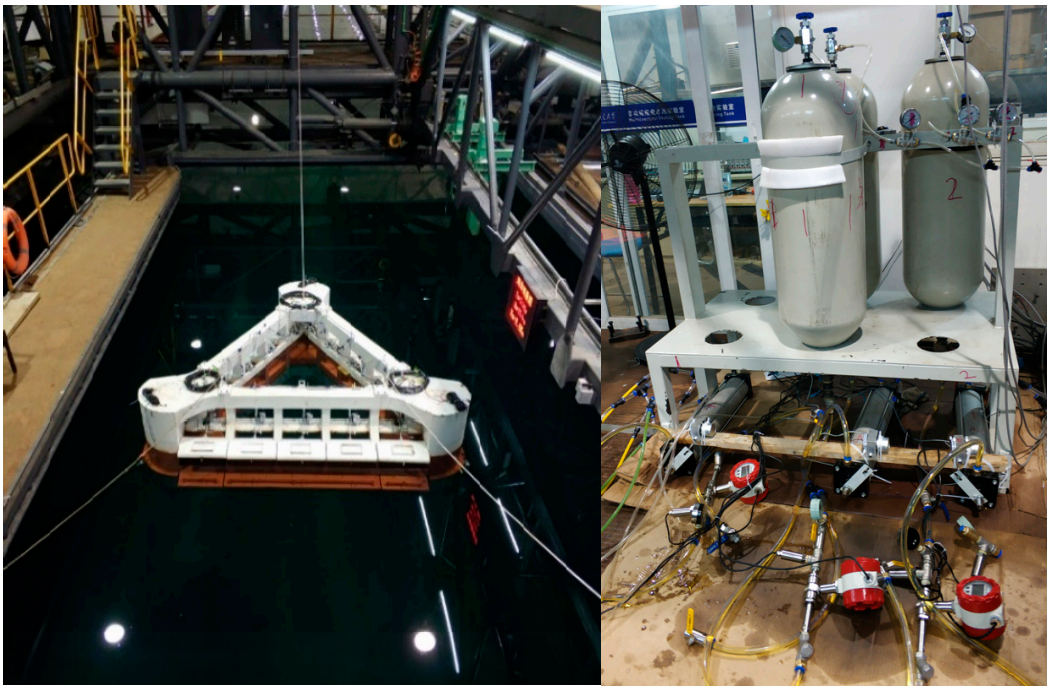

(**a**) (**b**)

Figure 3. 1 MW WEC 1:25 model: (**a**) 1 MW WEC 1:25 model in the towing tank; (**b**) the hydraulic energy conversion system used in the 1:25 scale model test.

In the experiments, each sharp eagle-shaped wave absorber, hinged to the platform via support rods at its rear end, underwent reciprocating rotation about pivot points. Wave crests drove the wave absorber motion, activating the hydraulic cylinders to convert wave energy into mechanical energy. The hydraulic cylinders compressed and discharged hydraulic oil and transformed mechanical energy into hydraulic energy. In the 1:25 scale model test, an equivalent energy conversion measurement system was employed to simulate the power capture characteristics of the full-scale prototype's hydraulic-to-electrical conversion (Stage III). Within this scaled system, hydraulic oil compression was converted and stored as pneumatic energy in compressed air units. It must be emphasized that this pneumatic approach was implemented exclusively for laboratory-scale modeling to facilitate convenient simulation and measurement of the Power Take-Off (PTO) system's damping characteristics, whereas the full-scale prototype Nankun directly utilizes the aforementioned hydraulic-to-electrical conversion system. Figure 3b shows the hydraulic energy conversion system of the WEC model.

In Figure 4, the beginning and end of the tank are wave making and absorption systems, respectively. A three-chain mooring system connected the model to the tank floor, restricting horizontal offset to within operational limits. The model layout in the tank allowed wave direction variation via rotation. Wave direction is defined as follows: 180 deg, waves incident on the platform's beam, with wave absorbers 6–10 facing head-on; 0 deg, bow-column heading waves.

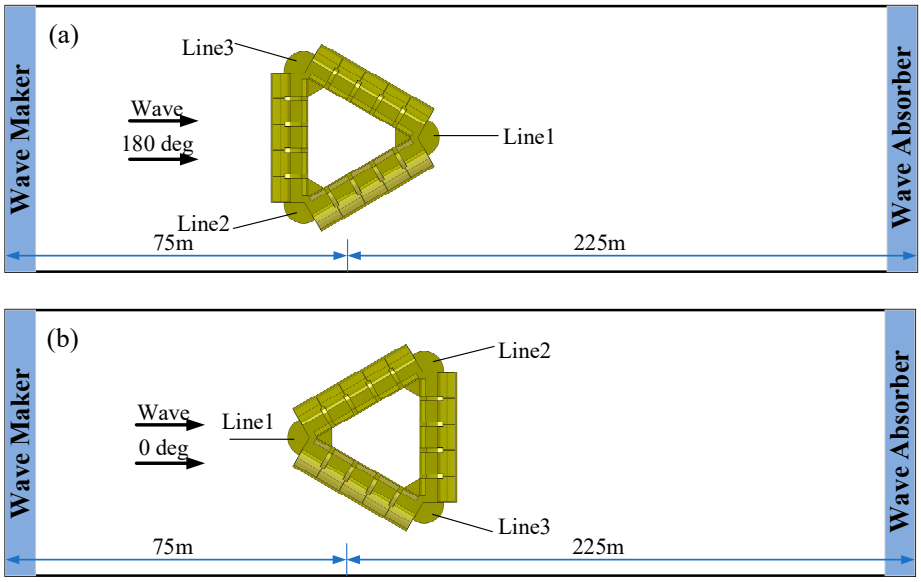

Figure 4. Plan view of 1 MW WEC 1:25 model in the towing tank: (**a**) wave direction of 180 deg; (**b**) wave direction of 0 deg.

3.3. Measurement System

Fifteen integrated tension–compression force sensors and displacement sensors were applied to measure the hydraulic cylinder force and displacement at each wave absorber's rear end, as shown in Figures 5 and 6. The force sensor has a measurement range of 0 to 100 N with an accuracy of ±0.1% FS (full scale), while the displacement sensor is rated at a 0–1000 mm range with a ±0.5% FS accuracy. Wave parameters were monitored using two capacitive wave gauges, while a digital HD camera recorded all the test process. All the instruments were calibrated pre-testing to ensure accuracy and reliability of the measurements. Tests employed 120 s wave durations per condition to achieve statistical stationarity.

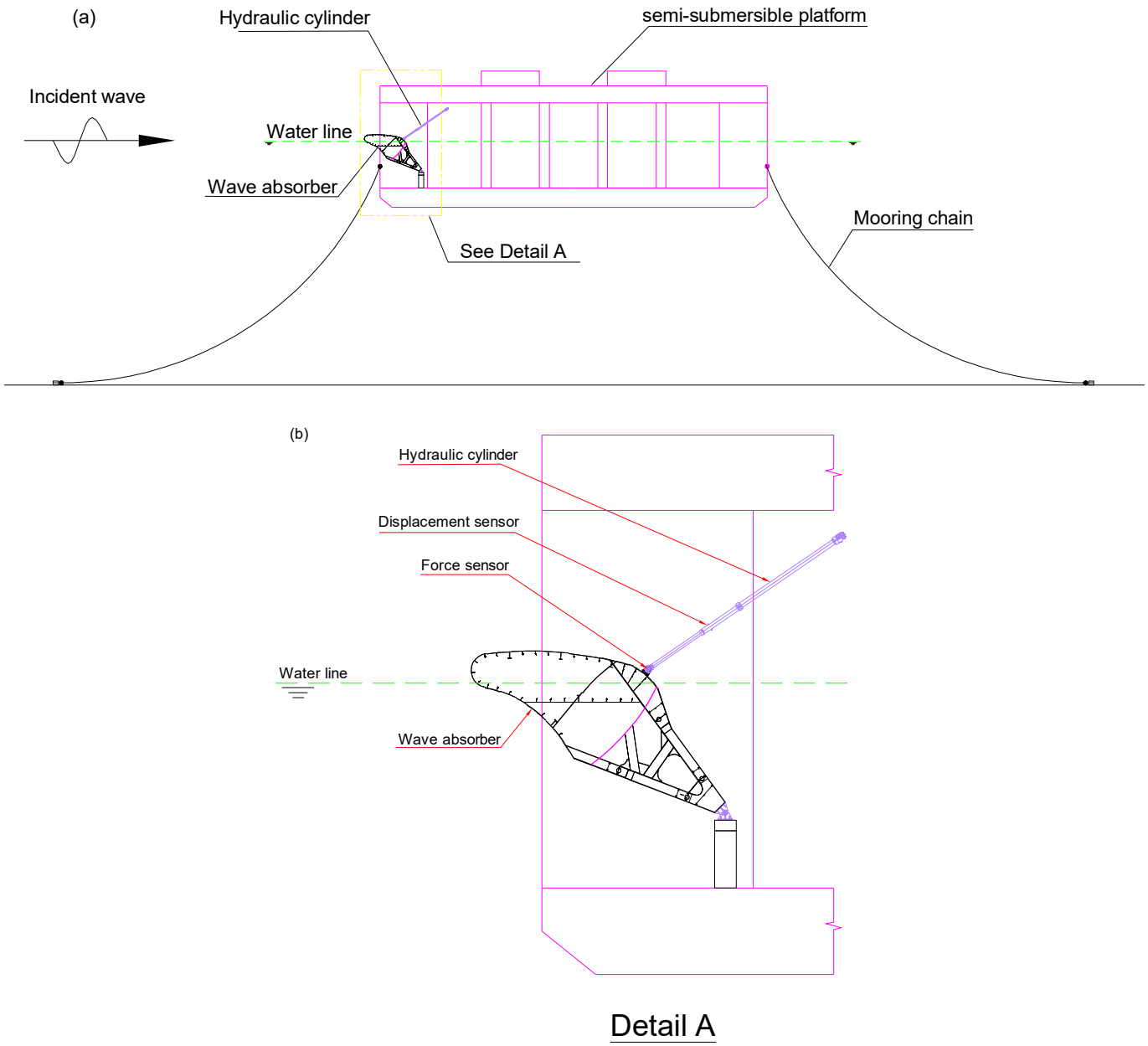

Figure 5. Diagram of the instrument setup: (**a**) overall layout diagram; (**b**) enlarged detail view.

3.4. Test Conditions

The 1 MW WEC is designed for optimal power generation in sea states with wave heights of 0.75–3 m and wave periods of 4–10 s. To evaluate its hydrodynamic performance, test conditions targeted prototype-equivalent sea states. Scaled regular waves (wave height: 30–120 mm, wave period: 0.8–2 s) were generated at wave directions of 180 deg and 0 deg. Test conditions are listed in Table 4. Cases 1–6 examine energy-capture efficiency under varying wave heights (30–120 mm) at constant periods (0.8–1.4 s) for 180 deg waves. Case 7 characterizes wave period sensitivity (0.8–2.0 s) at a fixed wave height (60 mm) for 180 deg waves. Cases 8–10 quantify wave direction effects by comparing the 0 deg performance against equivalent 180 deg conditions. To ensure data reliability, each wave condition (i.e., combination of wave height and period) was repeated in three independent tests, and the final result was presented as the arithmetic mean.

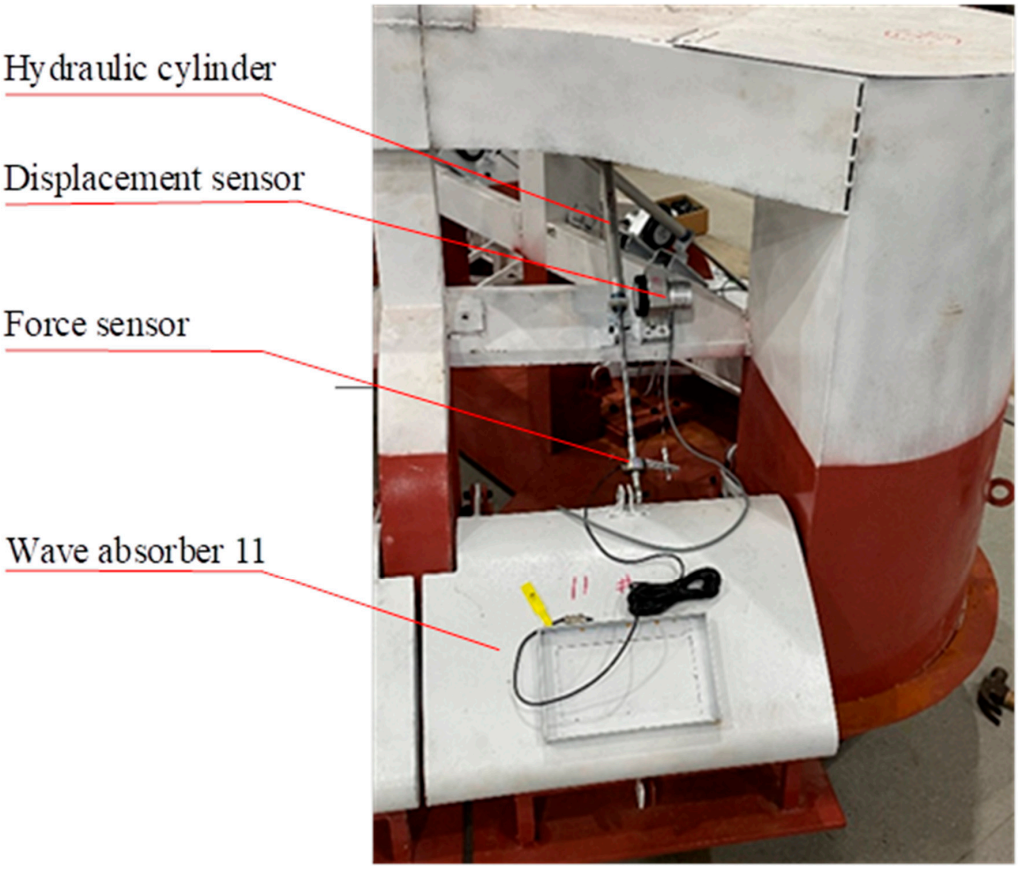

Figure 6. The instrument setup in the tests.

Table 4. Experimental test conditions.

Case	Wave Direction (deg)	Wave Height H (mm)	Wave Period T (s)
1–6	180	30, 40, 50, 60, 70, 80	0.8
	180	30, 40, 50, 60, 70, 80, 90	0.9
	180	40, 50, 60, 70, 80, 90	1.0
	180	40, 50, 60, 70, 80, 90, 100, 110	1.1
	180	50, 60, 70, 80, 90, 100, 110	1.2
	180	50, 60, 70, 80, 90, 100, 110, 120	1.4
7	180	60	0.8, 0.9, 1.0, 1.1, 1.2, 1.4, 1.6, 1.8, 2.0
8–10	0	60	0.8, 1.0
	0	70	0.9
	0	80	1.1, 1.2

4. Results and Discussion of Model Test

4.1. Energy-Capture Efficiency Methodology

Experimental investigations quantified the energy-capture performance of the 1 MW WEC under regular wave conditions. The system's fifteen sharp eagle-shaped wave absorbers convert incident wave energy into hydraulic cylinder kinetic energy. Energy-capture efficiency in regular waves is defined as follows:

$$\eta = \frac{P_c}{P_w} \tag{1}$$

where P_c is the captured power:

$$P_c = FS/t \tag{2}$$

and P_w the incident wave power [43]:

$$\begin{aligned} P_w &= \rho g H^2 \tfrac{\omega}{16k}[1 + 2kh/\sinh(2kh)]b \\ &= \rho g H^2 \tfrac{L}{16T}[1 + 2kh/\sinh(2kh)]b \end{aligned} \quad (3)$$

Here, F denotes the hydraulic cylinder force; S the hydraulic cylinder displacement; t the measurement duration; ρ the water density 1000 kg/m^3; g the gravitational acceleration; H the wave height; ω the wave frequency, $\omega = 2\pi/T$; T the wave period; k the wave number, $k = 2\pi/L$; L the wave length; h the water depth; and b the projected width of the absorber normal to wave direction.

Therefore,

$$\eta = \frac{P_c}{P_w} = \frac{FS/t}{\rho g H^2 \frac{L}{16T}[1 + 2kh/\sinh(2kh)]b} \times 100\% \quad (4)$$

4.2. Energy-Capture Performance

The sharp eagle-shaped wave absorbers convert incident wave energy into reciprocating motions of the hydraulic cylinders. Figure 7 illustrates the force–displacement relationship for wave absorber 6's hydraulic cylinder under 180 deg wave direction, H = 70 mm, and T = 1.0 s, revealing two distinct operational phases. In the compression phase, wave crests drive an upward absorber motion, applying a compressive force (negative values) that reduces the piston displacement from the equilibrium. The initial piston displacement in the equilibrium position is 123.8 mm. In the tension phase, wave troughs induce a downward absorber motion, generating a tensile force (positive values) that increases the piston displacement.

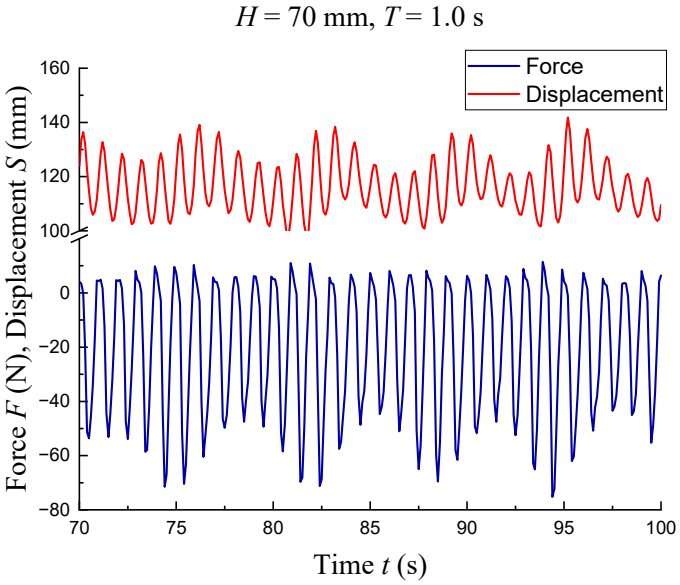

Figure 7. Force and displacement for wave absorber 6's hydraulic cylinder, under 180 deg wave direction, H = 70 mm, and T = 1.0 s.

Compute work in upward motion per wave absorber through force–displacement integration over 30 stable cycles. This is the captured power per wave absorber. By calculating absorber efficiency using Equation (1), then summing contributions from all 15 wave absorbers, the system's total energy-capture efficiency is thus obtained.

Experimental results of wave energy captured in 180 deg wave direction are presented in Table 5. The results represent the mean of 3 repeated tests. During the test, the system's fifteen wave absorbers simultaneously actuated the rear hydraulic cylinders. The total energy-capture efficiency of the 1 MW WEC's absorbers typically ranges between 30% and

50%. At a constant wave period, the efficiency initially increases and then decreases with increasing wave height. The motion response of the WEC is significantly influenced by both wave period and height. Under the condition of H = 50 mm and T = 1.0 s, the WEC exhibits optimal motion response and peak capture ability, achieving a maximum capture efficiency of approximately 56.17%.

Table 5. Total energy-capture efficiency in 180 deg wave direction.

***H*(m)/*T*(s)**	**0.8**	**0.9**	**1**	**1.1**	**1.2**	**1.4**
30	38.69%	28.56%				
40	41.23%	26.85%	50.30%	30.89%		
50	42.00%	29.53%	56.17%	35.19%	30.71%	33.67%
60	43.05%	33.34%	50.54%	38.97%	39.41%	44.97%
70	27.82%	37.91%	46.30%	42.50%	39.61%	46.44%
80	16.47%	36.60%	43.74%	42.59%	40.41%	47.06%
90		27.10%	38.63%	38.32%	36.54%	43.14%
100				41.52%	38.87%	32.39%
110				36.67%	33.32%	29.31%
120						30.26%

The sharp eagle shape, width, and mass of the wave absorber were specifically optimized during the preliminary design phase to achieve a natural period of pitch resonance close to 5.0 s. This value was chosen because it matches the most energetic and frequently occurring wave periods at the target deployment site, thereby maximizing the potential for resonant energy capture. And the natural period of pitch motion for a single wave absorber of the final-design 1 MW WEC was 4.83 s. The optimal condition revealed by the test results is closely related to the design parameters of the device. The observed optimal period T = 1.0 s in the model tests is directly linked to the natural period of pitch motion of the wave absorbers. Through Froude scaling (with a scale factor of $\lambda = 25$), this corresponds to a full-scale period of 5 s. This is very close to the natural period of pitch motion of the prototype 1 MW WEC, which is 4.83 s. The optimal wave height H = 50 mm in the model represents a balance. For wave heights significantly lower than this, wave excitation force is insufficient to overcome the Power Take-Off system's stiction and the threshold pressure, leading to very low efficiency. Conversely, for wave heights significantly larger than the optimum, several factors can reduce efficiency: (1) The motion of the absorber may exceed the designed maximum stroke length of the hydraulic cylinders, leading to mechanical end-stop impacts and a loss of captured energy. (2) Highly nonlinear hydrodynamic effects, such as wave overtopping and slamming, can occur, which alter the pressure distribution on the absorber and can reduce the effective relative motion between the absorber and the platform. Consequently, the optimal wave period T = 1.0 s and height H = 50 mm (corresponding to 5.0 s and 1.25 m at a full-scale height), represent the wave condition where the system exhibits its most favorable motion response and achieves peak energy-capture efficiency.

The results show that the 1 MW WEC Nankun has a capture efficiency greater than 30% under most wave conditions, and it has a maximum capture efficiency of 56.17%, which is much higher than that of the other major WECs in Table 1. The greatest advantage of Nankun is that it is equipped with multiple wave absorbers, which enhances the energy capture density and quality. It achieves improvements in cost-effectiveness through the shared semi-submersible platform. Also, the three-sided wave-absorber array has inherent advantages when facing multidirectional waves.

Figure 8 presents the energy-capture efficiency of the WEC. The red dots represent the total efficiency, while the brown, blue, and green dots denote respective group efficiencies

of the three-sided wave-absorber array. The data points in the figure represent the mean of three repeated tests, and the error bars represent the standard deviation. The generally short length of the error bars across the various conditions indicates that the experimental data has good consistency and repeatability. The red line indicates the fitted total efficiency, and the blue curve shows the fitted efficiency for wave absorbers 6–10.

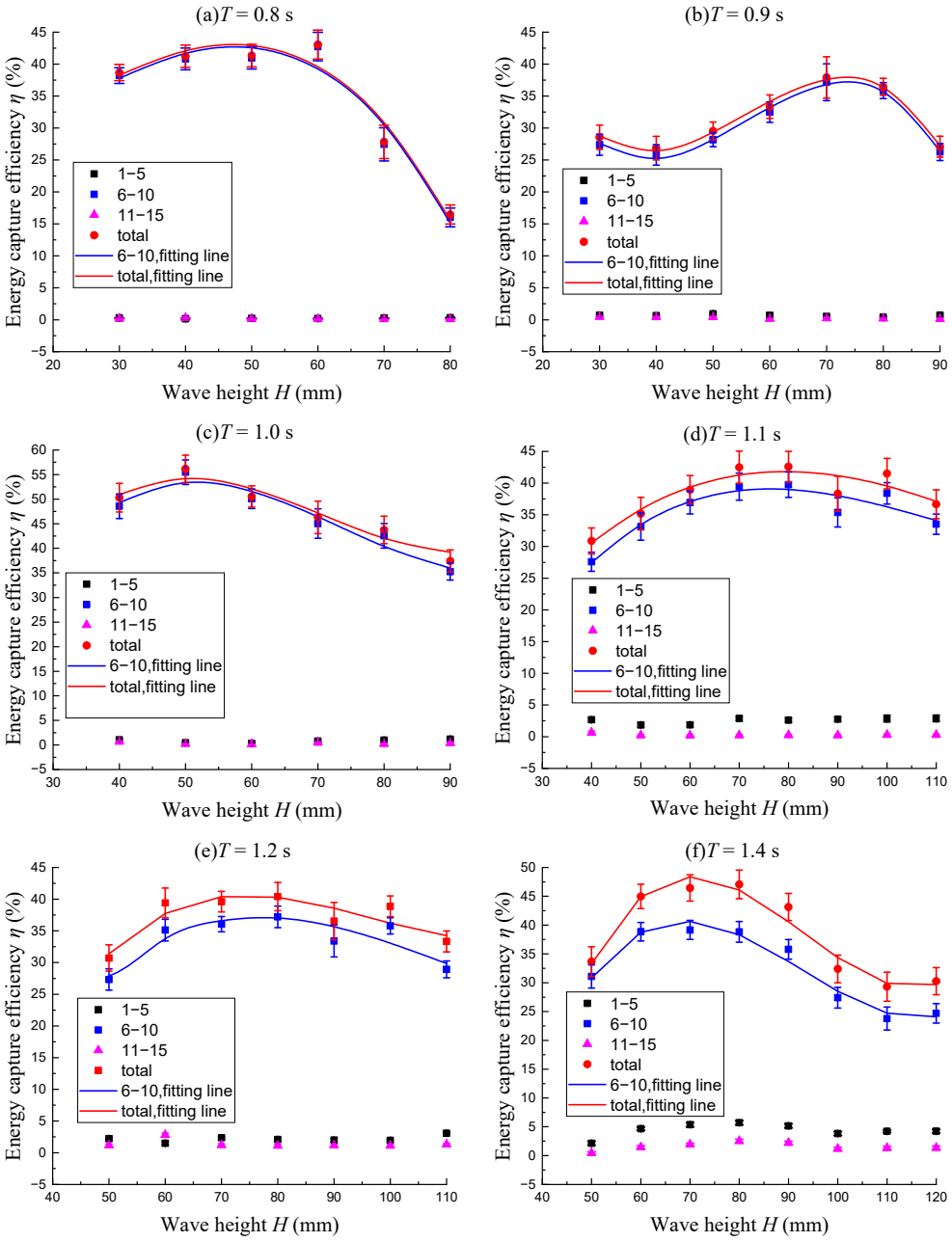

Figure 8. Energy-capture efficiency in 180 deg wave direction.

As shown in Figure 8, the total wave energy-capture efficiency exhibits a distinct inverted U-shaped trend with respect to wave height. Specifically, efficiency rises as height increases from 30 mm to approximately 60 mm, but declines when height increases further from approximately 70 mm to 120 mm. Consequently, the optimal wave height range for efficiency is found to be between 40 mm and 70 mm, where efficiency mostly exceeds 40%. This optimal model-scale range corresponds to prototype wave heights of 1.0 m to 1.75 m.

Figure 8 further depicts the total energy-capture efficiency of the WEC along with respective group efficiencies of the three-sided wave-absorber array under 180 deg wave

direction. At shorter wave periods of 0.8–1.0 s, the total energy-capture efficiency is predominantly contributed (>95%) by the centrally positioned absorbers 6–10, with the starboard and port lateral absorbers 1–5 and 11–15 exhibiting minimal motion and contributing to only 5% of total efficiency. At longer periods of 1.1–1.4 s, the central absorbers 6–10 maintain high contribution levels (82–94%), while lateral absorbers account for 6–18% of total efficiency. Wave absorber performance exhibited strong positional dependence. Central absorbers 6–10 directly intercept undisturbed incident waves at the semi-submersible platform's wave-facing front (180 deg heading), maximizing energy capture. Lateral absorbers 1–5 and 11–15 reside in the sheltered zones, capturing attenuated energy from diffracted waves. The diffraction effect is significantly weaker at shorter wave periods, reducing energy availability for lateral absorbers. Hence their efficiency at periods of 0.8–1.0 s is smaller than that of periods of 1.1–1.4 s.

Despite symmetrical arrangement, lateral absorbers exhibit 4–10% inter-group efficiency variance in Figure 8d–f. This asymmetry stems from installation tolerances in hydraulic systems coupled with wake interference effects. Minor variations in hydraulic cylinder and piping alignment perturb individual absorber kinematics, particularly under longer wave periods where flow dynamics dominate. Concurrently, asymmetric vortex shedding from central absorbers 6–10 generates differential flow conditions for starboard 1–5 and port 11–15 absorber groups, further amplifying efficiency discrepancies.

4.3. Wave Period Effect

Figure 9 depicts the wave energy-capture efficiency under 180 deg wave heading at a fixed wave height of 60 mm across varying wave periods. The WEC exhibits broad spectral responsiveness, maintaining a high capture efficiency (>30%) within the 0.8–1.4 s period range which covers typical wave energy resource bands. Peak efficiency occurs at periods of 0.8 s, 1.0 s, and 1.4 s, while a significant reduction is observed beyond 1.6 s.

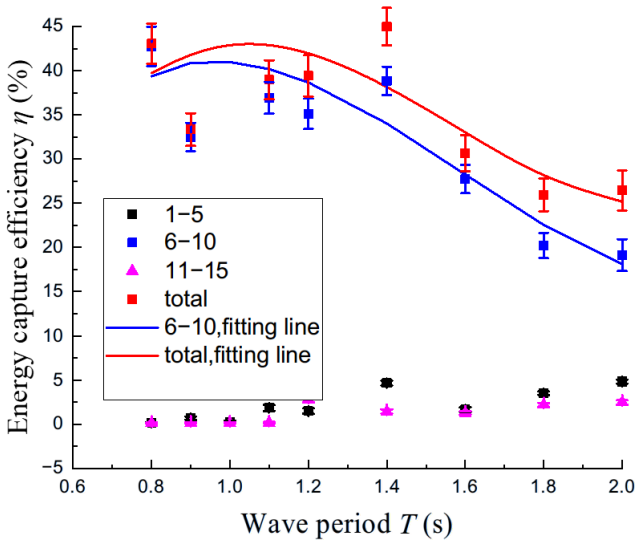

Figure 9. Energy-capture efficiency in 180 deg wave direction at a fixed wave height of 60 mm across varying wave periods.

4.4. Wave Direction Effect

Energy-capture efficiency of the 1 MW WEC under 0 deg wave direction are presented in Table 6. Total efficiency ranges primarily between 20% and 35%, with wave energy predominantly captured by starboard 1–5 and port 11–15 absorber groups. The starboard and port efficiencies exhibit approximate parity, while aft central absorbers 6–10 contribute negligibly (<5% total efficiency) due to wave shadowing effects from the

bow column, experiencing obvious wave height attenuation behind the forward structure during the tests.

Table 6. Energy-capture efficiency in 0 deg wave direction.

Wave Period *T* (s)	Wave Height *H* (mm)	Efficiency			
		Total	1–5	6–10	11–15
0.8	60	23.43%	12.68%	0.21%	10.54%
0.9	70	26.80%	12.91%	0.17%	13.72%
1.0	60	24.71%	12.62%	0.14%	11.95%
1.1	80	29.01%	13.83%	0.09%	15.09%
1.2	80	33.63%	16.33%	0.07%	17.23%

Energy-capture performance response to wave direction was quantified by comparing the efficiency at 0 deg and 180 deg wave headings under equivalent wave parameters (H = 60–80 mm, T = 0.8–1.2 s). Table 7 illustrates the relative efficiency ratio between 0 deg and 180 deg across tested conditions, revealing directional anisotropy. Compared with 180 deg wave direction, energy-capture efficiency is smaller in the 0 deg wave direction under the same wave period and height. The efficiency of the 0 deg wave direction is only about 60–80% of that of the 180 deg in most wave conditions. This efficiency deficit arises from fundamental wave–structure interactions. At 0 deg, lateral absorbers 1–5 and 11–15 face incident waves sideways, reducing effective capture width. The aft central absorbers 6–10 are hydrodynamically shielded in the wave shadowing area. At 180 deg, central absorbers 6–10 receive direct wave excitation, maximizing energy capture. These results validate the central absorbers configuration's optimization for beam seas, suggesting preferential deployment in prevailing wave climates with dominant directionality. For omnidirectional sites, absorber redistribution or platform rotation control should be considered to mitigate efficiency losses.

Table 7. Energy-capture efficiency in 0 deg vs. 180 deg wave directions.

Wave Period *T* (s)	Wave Height *H* (mm)	Total Efficiency		Relative Efficiency Ratio
		Wave Direction 0 deg	Wave Direction 180 deg	
0.8	60	23.43%	43.05%	0.54:1
0.9	70	26.80%	37.91%	0.71:1
1.0	60	24.71%	50.54%	0.49:1
1.1	80	29.01%	42.59%	0.68:1
1.2	80	33.63%	40.41%	0.83:1

While the present study establishes the device's energy-capture performance in head (0 deg) and beam (180 deg) seas, a comprehensive investigation into its dynamic response and energy efficiency across a full range of intermediate wave angles (e.g., 30 deg, 45 deg, 90 deg, etc.) is a crucial next step for future work.

5. Construction and Sea Trial

The 1 MW WEC Nankun was constructed at the COSCO Shipping Heavy Industry and deployed in the South China Sea for the sea trial in 2023, shown as Figure 10. The water depth at this site is approximately 40 m, and the seabed topography is relatively flat, with a sandy bottom. The site is a weak-tide sea area. The average monthly tidal range over the past three years is only 92 cm, and the annual average of the maximum monthly tidal range is only 159.9 cm. According to historical data, the wave climate characteristics of this sea area are as follows: the annual average wave height is approximately 1.52 m; the period is mainly distributed between 4.5 and 6.0 s; the prevailing wave direction is from the northeast; and the secondary prevailing direction is from the southwest. The design parameters of Nankun, particularly the natural period of the wave absorber, are optimized

specifically for this typical wave climate. At the sea trial site, one side of the triangular platform faced toward the island with negligible wave incidence. To optimize structural efficiency, the triangular platform's wave absorbers were reconfigured: 5 absorbers on the leeward-facing Side C were omitted, while 10 absorbers on primary wave-facing Sides A and B were retained.

(**a**) (**b**)

Figure 10. 1 MW WEC Nankun in sea trial: (**a**) front view; (**b**) plan view.

Table 8 summarizes the principal specifications and configuration of the 1 MW WEC Nankun. Its hydraulic energy conversion system comprises four identical independent sets, each set structured with six core modules: a hydraulic power module, energy storage and pressure stabilization module, power generation module, condition monitoring module, high-pressure oil tank module, hydraulic piping network, and auxiliary components. Each hydraulic power module integrates five 6.7 m-stroke hydraulic cylinders (20 hydraulic cylinders total, system-wide). Dual cylinders are connected per wave absorber. Each power generation module employs a hybrid configuration of one 150 kW and two 50 kW generators. Aggregating across four sets yields the rated 1 MW installed capacity. All hydraulic generator units are rectified, and their outputs are consolidated onto a 750 V DC bus. A dedicated grid-connected inverter then delivers the power to the utility grid. The inverter ensures stable grid integration of the 1 MW WEC Nankun by actively tracking the grid's voltage and frequency.

Table 8. Technical specifications of the prototype 1 MW WEC Nankun.

System	Parameter	Value
Platform	Dimensions	88 m × 80 m × 24 m
	Operational draft	13.5 m
	Survival draft	16.5 m
	Operational displacement	13,229 t
	Survival displacement	15,720 t
Mooring system	Configuration	3 × 2 lines (R3S chain, diameter 107 mm, 650 m length).
	Anchor type	6 × 30 t drag embedment anchor.
Wave energy capture system	Absorbers	10 sharp eagle-shaped wave absorbers on Sides A and B.
	Width of an absorber	11.7 m
Hydraulic energy conversion system	Hydraulic power module	4 sets, symmetric distribution on Sides A and B, named AX, AY, BX, BY.
	Hydraulic cylinder	5 cylinders per module, designed stroke length of 6.7 m.
	Generator	4 sets, each set consists of one 150 kW and two 50 kW generators.
Ancillary Systems	Solar PV	250 kW
	Battery storage	560 kWh
	Diesel generator	Main power supply 350 kW, emergency power supply 200 kW.

The sea trial site experiences prevailing northeasterly winter waves. The 1 MW WEC Nankun was oriented with Side A facing northeast (primary wave incidence) and Side B facing west (leeward orientation). Following on-site positioning and commissioning

completion in November 2023, grid connection and power supply was achieved via the pre-installed submarine cable.

During operations, wave absorbers autonomously start to capture wave energy as wave height reaches 0.5 m, then converts hydraulic energy storage into electricity. Safety protocols trigger wave energy capture system cut-out when wave height exceeds 5.0 m. Figure 11 documents daily power generation from 1–20 November 2023, coinciding with the northeast monsoon period. Enhanced wave energy resources during this phase resulted in daily energy yields exceeding 4000 kWh on 12 of the 20 monitored days. The peak daily output of 9850 kWh recorded on 15 November 2003 satisfies the daily electricity demand of an island with a population of approximately 1000 residents.

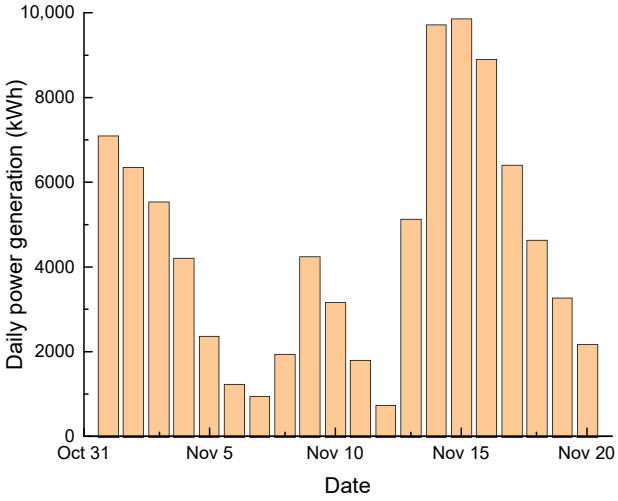

Figure 11. Daily power generation profile of 1 MW WEC *Nankun* during sea trial.

Figure 12 presents the hourly averaged power output of the 1 MW WEC Nankun during the 20-day monitoring period (from 1 to 20 November 2023). A strong correlation exists between the average output power and daily power generation profile. High average output power is consistently observed on days of high daily energy yield, such as on 1–4, 9, and 13–18 November. The peak output power of 464.6 kW occurred at 21:00 on 13 November 2023. Cumulative power generation over this period reached 89,852 kWh as shown in Figure 13.

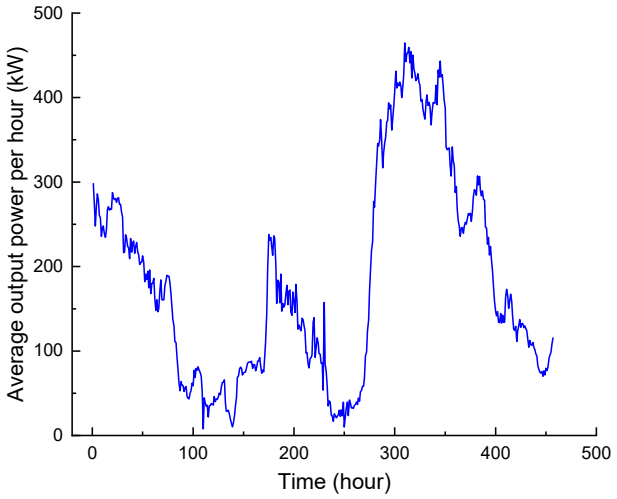

Figure 12. Average output power per hour of 1 MW WEC *Nankun*.

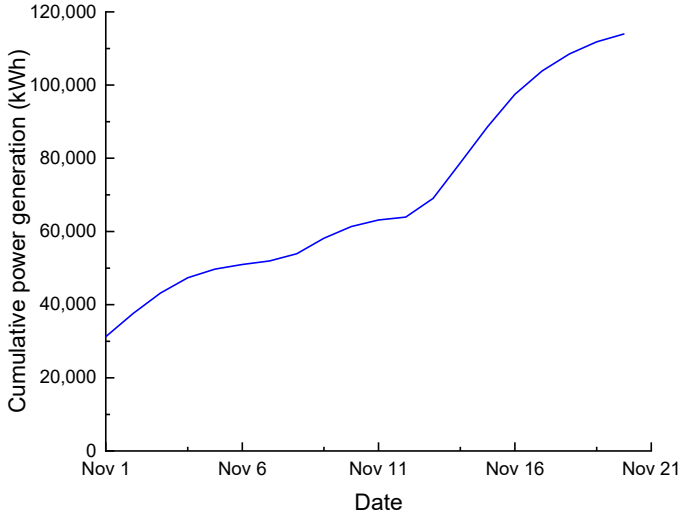

Figure 13. Cumulative power generation.

It is important to acknowledge the limitations of the data collected during this inaugural sea trial, which were significantly impacted by the timing and conditions of the deployment. The trial commenced in late autumn and was shortly followed by a severe winter period where sea states exceeded the device's operational wave height limit of 5 m. This led to extended periods of protective downtime, complicating the collection of continuous operational data. As this was the inaugural deployment, the primary focus was on validating the fundamental power generation performance. A comprehensive assessment of long-term reliability metrics, such as system availability, capacity factor, and failure frequency, was not completed. Furthermore, these severe weather conditions compromised our efforts to collect concurrent environmental data. Wave data measured on-site are not reliable enough for a rigorous comparative analysis of the device's efficiency. Consequently, the primary objective for the next phase of sea trials is to implement a more robust data acquisition strategy, encompassing both the systematic collection of these crucial operational indicators and the resilient deployment of in situ wave measurement systems. This will enable a comprehensive validation of the device's performance and reliability against real-sea conditions.

6. Conclusions

This study presents the complete development process, from conceptual design and scaled-model testing to full-scale offshore deployment, of an innovative multi-absorber 1 MW WEC. Laboratory experiments were conducted to investigate the energy-capture performance of the device in wave conditions, with emphasis on wave height, period, and directional effects. A full-scale prototype with 10 absorbers was deployed in the South China Sea, achieving grid connection in November 2023. The main conclusions are drawn as follows:

(1) Model tests demonstrate that the device has energy capture efficiencies of 30–50% within the 0.8–1.4 s wave period range. In the 180 deg wave direction, efficiency exhibits an inverted-U trend with wave height, peaking at 56.17% under optimal wave condition (wave height 50 mm, period of 1.0 s). The optimal wave period of 1.0 s is scaled up to the full-scale prototype period of 5 s, which corresponds to the natural period of 4.83 s of pitch motion for a single wave absorber of the final-designed 1 MW WEC.

(2) In the 180 deg wave direction, frontally aligned central absorbers 6–10 capture over 80% of incident wave energy, while rear and lateral absorbers 1–5 and 11–15 contribute

minimally due to hydrodynamic shadowing effects. Wave absorber performance exhibited strong positional dependence. Therefore, five wave absorbers on Side C facing the island have been canceled. The 1 MW WEC Nankun was oriented with Side A facing northeast (predominant northeasterly winter waves) and Side B facing west (predominant southwesterly summer waves).

(3) The WEC maintains a high capture efficiency (>30%) within the 0.8–1.4 s period range. Peak efficiency occurs at periods of 0.8 s, 1.0 s, and 1.4 s, with efficiency declining beyond 1.6 s.

(4) The device achieves significantly higher energy capture at 180 deg versus 0 deg wave headings, with an efficiency ratio of approximately 1.0:0.6~0.8. Orienting wave absorbers towards predominant wave directions maximizes energy capture.

(5) 1 MW WEC Nankun generated 89,852 kWh cumulatively, with a peak daily output of 9850 kWh and a maximum power of 464.6 kW over a 20-day operational window. Field operational data validate the technical viability of MW-grade WEC for remote island applications.

Although this study has achieved positive results, there are still some limitations that require future work to address. First, the current operational data only covers a few months; longer-term (e.g., multi-year) continuous monitoring is needed to fully assess the device's long-term reliability, material fatigue characteristics, and survivability in extreme sea conditions. Second, the existing PTO control strategy has room for optimization. Further research could investigate advanced algorithms based on model predictive control to enhance energy-capture efficiency across a wider range of sea states. Finally, to improve the versatility of this design for different climatic and geomorphological settings, a key future task will be to develop a high-fidelity numerical model validated by field data. This model will be able to simulate the device's performance in different wave climates and guide the optimization of design parameters for specific sites, thereby promoting the technology towards broader commercial application.

Author Contributions: Conceptualization, M.C., S.S. and K.W.; methodology, M.C., S.S. and Y.Z.; software, M.C. and Y.Z.; validation, M.C., Z.W. and J.J.; formal analysis, M.C. and Y.Z.; investigation, M.C. and Y.Z.; resources, S.S.; data curation, M.C.; writing—original draft preparation, M.C.; writing—review and editing, S.S., Z.W. and K.W.; visualization, M.C.; supervision, S.S.; project administration, S.S.; funding acquisition, M.C. and S.S. All authors have read and agreed to the published version of the manuscript.

Funding: This research was supported by the Strategic Priority Research Program of the Chinese Academy of Sciences, Grant No. XDC0190201; President's Young Talent Cultivation Fund, Guangzhou Branch of the Chinese Academy of Sciences, Grant No. E590020201.

Data Availability Statement: The data presented in this study are available on request from the corresponding authors.

Conflicts of Interest: The authors declare no conflicts of interest.

References

1. Leonard, M.D.; Michaelides, E.E.; Michaelides, D.N. Energy storage needs for the substitution of fossil fuel power plants with renewables. *Renew. Energy* **2020**, *145*, 951–962. [CrossRef]
2. Lu, Y.; Khan, Z.; Alvarez-Alvarado, M.; Zhang, Y.; Huang, Z.; Imran, M. A critical review of sustainable energy policies for the promotion of renewable energy sources. *Sustainability* **2020**, *12*, 5078. [CrossRef]
3. Falnes, J. A review of wave-energy extraction. *Mar. Struct.* **2007**, *20*, 185–201. [CrossRef]
4. Rodrigues, C.; Nunes, D.; Clemente, D.; Mathias, N.; Correia, J.M.; Rosa-Santos, P.; Taveira-Pinto, F.; Morais, T.; Pereira, A.; Ventura, J. Emerging triboelectric nanogenerators for ocean wave energy harvesting: State of the art and future perspectives. *Energy Environ. Sci.* **2020**, *13*, 2657–2683. [CrossRef]

5. Clément, A.; McCullen, P.; Falcão, A.; Fiorentino, A.; Gardner, F.; Hammarlund, K.; Lemonis, G.; Lewis, T.; Nielsen, K.; Petroncini, S.; et al. Wave energy in Europe: Current status and perspectives. *Renew. Sustain. Energy Rev.* **2002**, *6*, 405–431. [CrossRef]
6. Cruz, J. *Ocean Wave Energy: Current Status and Future Perspectives*; Springer: Berlin, Germany, 2008.
7. Wu, H.; Fang, Y.; Zhang, S.; Ma, Y. Wave energy characterization and potential estimation for islands of South China Sea. *Acta Energ. Sol. Sin.* **2022**, *43*, 416–423.
8. Falcão, A.F.O. Wave energy utilization: A review of the technologies. *Renew. Sustain. Energy Rev.* **2010**, *14*, 899–918. [CrossRef]
9. Drew, B.; Plummer, A.R.; Sahinkaya, M. A review of wave energy converter technology. *Proc. Inst. Mech. Eng. Part. A J. Power Energy* **2009**, *223*, 887–902. [CrossRef]
10. Thorpe, T. An overview of wave energy technologies: Status, performance and costs. In *Wave Power: Moving Towards Commercial Viability*; Broadway House: Westminster, UK, 1999.
11. Fredriksen, A.E. Tapered Channel Wave Power Plants. In Proceedings of the Fourth International Conference on Energy for Rural and Island Communities, Inverness, Scotland, 16–19 September 1985.
12. Kofoed, J.P.; Frigaard, P.; Friis-Madsen, E.; Sørensen, H.C. Prototype testing of the wave energy converter wave dragon. *Renew. Energy* **2006**, *31*, 181–189. [CrossRef]
13. Tedd, J.; Kofoed, J.P. Measurements of overtopping flow time series on the Wave Dragon, wave energy converter. *Renew. Energy* **2009**, *34*, 711–717. [CrossRef]
14. Jasinski, M.; Malinowski, M.; Kazmierkowski, M.P.; Sørensen, H.C.; Friis-Madsen, E.; Swierczynski, D. Control of AC/DC/AC converter for multi MW wave dragon offshore energy conversion system. In Proceedings of the IEEE International Symposium on Industrial Electronics, Vigo, Spain, 4–7 June 2007.
15. Hur, D.S.; Jeong, Y.M.; Lee, J.L.; Kim, I.H.; Lee, W.D. Energy generation efficiency due to wave overtopping on floating-overflow-type wave energy converter. *J. Coast. Res.* **2018**, *85*, 1341–1345. [CrossRef]
16. Kim, J.; Park, M.S.; Jeong, Y.J. Integration analysis and evaluation of new hybrid 3kW ocean wave energy extraction system. *J. Coast. Res.* **2018**, *85*, 1316–1320. [CrossRef]
17. Vicinanza, D.; Frigaard, P. Wave pressure acting on a seawave slot-cone generator. *Coast. Eng.* **2008**, *55*, 553–568. [CrossRef]
18. Margheritini, L.; Vicinanza, D.; Frigaard, P. SSG wave energy converter: Design, reliability and hydraulic performance of an innovative overtopping device. *Renew. Energy* **2009**, *34*, 1371–1380. [CrossRef]
19. Vicinanza, D.; Margheritini, L.; Kofoed, J.P.; Buccino, M. The SSG wave energy converter: Performance, status and recent developments. *Energies* **2012**, *5*, 193–226. [CrossRef]
20. Tanaka, H.; Inami, T.; Sakurada, T. Characteristics of volume of overtopping and water supply quantity for developing wave overtopping type wave power generation equipment. In Proceedings of the 25th International Ocean and Polar Engineering Conference, Kona, HI, USA, 21–26 June 2015.
21. Kim, J.S.; Nam, B.W.; Kim, S.; Park, J.; Park, S.; Kim, K.H. Experimental study on hydrodynamic behavior and energy conversion of multiple oscillating-water-column chamber in regular waves. *Ocean Eng.* **2023**, *280*, 114495. [CrossRef]
22. Barnard, C. *The Whistling Buoy*; Kessinger Publishing: Whitefish, MT, USA, 1887.
23. Heath, T.V. A review of oscillating water columns. *Philos. Trans. R. Soc. A Math. Phys. Eng. Sci.* **2012**, *370*, 235–245. [CrossRef]
24. Falcão, A.F.O.; Henriques, J.C.C. Oscillating-water-column wave energy converters and air turbines: A review. *Renew. Energy* **2016**, *85*, 1391–1424. [CrossRef]
25. Guo, B.; Ringwood, J.V. A review of wave energy technology from a research and commercial perspective. *IET Renew. Power Gener.* **2021**, *15*, 3065–3090. [CrossRef]
26. Wu, B.; Chen, T.; Jiang, J.; Li, G.; Zhang, Y.; Ye, Y. Economic assessment of wave power boat based on the performance of "Mighty Whale" and BBDB. *Renew. Sustain. Energy Rev.* **2018**, *81*, 946–953. [CrossRef]
27. Lindroth, S.; Leijon, M. Offshore wave power measurements: A review. *Renew. Sustain. Energy Rev.* **2011**, *15*, 4274–4285. [CrossRef]
28. Falcão, A.F.O.; Henriques, J.C.C. Model-prototype similarity of oscillating-water-column wave energy converters. *Int. J. Mar. Energy* **2014**, *6*, 18–34. [CrossRef]
29. López, I.; Andreu, J.; Ceballos, S.; Alegría, I.M.; Kortabarria, I. Review of wave energy technologies and the necessary power-equipment. *Renew. Sustain. Energy Rev.* **2013**, *27*, 413–434. [CrossRef]
30. Hart, P.; Lurie, R. Application of PowerBuoy wave energy converter technology to remote power requirements in oil and gas field developments. In Proceedings of the Offshore Technology Conference, Houston, TX, USA, 30 April–3 May 2012.
31. Marquis, L.; Kramer, M.; Krimgelum, J.; Chozas, J.; Helstrup, N. Introduction of wavestar wave energy converters at the Danish offshore wind power plant Horns Rev 2. In Proceedings of the 4th International Conference on Ocean Energy, Dublin, Ireland, 17–19 October 2012.
32. Chozas, J.; Kramer, M.; Soerensen, H.; Kofoed, J. Combined production of a full-scale wave converter and a full-scale wind turbine-a real case study. In Proceedings of the 4th International Conference on Ocean Energy, Dublin, Ireland, 17–19 October 2012.

33. Whittaker, T.; Collier, D.; Folley, M.; Osterried, M.; Henry, A.; Crowley, M. The development of Oyster-a shallow water surging wave energy converter. In Proceedings of the 7th European Wave and Tidal Energy Conference, Porto, Portugal, 11–14 September 2007.
34. Henderson, R. Design, simulation, and testing of a novel hydraulic power take-off system for the Pelamis wave energy converter. *Renew. Energy* **2006**, *31*, 271–283. [CrossRef]
35. Bahaj, A.S. Generating electricity from the oceans. *Renew. Sustain. Energy Rev.* **2011**, *15*, 3399–3416. [CrossRef]
36. Sheng, S.W.; Zhang, Y.Q.; Wang, K.L.; Wang, Z.P.; Lin, H.J.; Ye, Y. Research on wave energy converter sharp eagle I. *Ship Eng.* **2015**, *37*, 104–108.
37. Sheng, S.W.; Wang, K.L.; Lin, H.J.; Zhang, Y.Q.; You, Y.G.; Wang, Z.P. Open sea tests of 100 kW wave energy convertor sharp eagle Wanshan. *Acta Energ. Sol. Sin.* **2019**, *40*, 709–714.
38. Sheng, S.W.; Wang, K.L.; Lin, H.J.; Zhang, Y.Q.; You, Y.G.; Wang, Z.P.; Chen, A.J.; Jiang, J.Q.; Wang, W.S.; Ye, Y. Model research and open sea tests of 100 kW wave energy convertor Sharp Eagle Wanshan. *Renew. Energy* **2017**, *113*, 587–595. [CrossRef]
39. AquaBuoy Wave Energy Converter. Available online: https://www.greencarcongress.com/2007/09/finavera-renewa.html (accessed on 1 September 2025).
40. Previsic, M. *Offshore Wave Energy Conversion Devices*; Electric Power Research Institute (EPRI) Report: Palo Alto, CA, USA, 2004.
41. Dalton, G.; Alcorn, R.; Lewis, T. Case study feasibility analysis of the Pelamis wave energy convertor in Ireland, Portugal and North America. *Renew. Energy* **2010**, *35*, 443–455. [CrossRef]
42. Renzi, E.; Dias, F. Resonant behaviour of an oscillating wave energy converter in a channel. *J. Fluid Mech.* **2012**, *701*, 482–510. [CrossRef]
43. Zou, Z.L. The wave theory in limited water depth. In *Water Wave Theores and Their Applications*, 1st ed.; Science Press: Beijing, China, 2005.